Korean J. Chem. Eng., 34(3), 885-891 (2017)
DOI: 10.1007/s11814-016-0323-z

pISSN: 0256-1115
eISSN: 1975-7220

Electrochemical properties of α-$Co(OH)_2$/graphene nano-flake thin film for use as a hybrid supercapacitor

En Mei Jin*, Hyeon Jeong Lee*, Hang-Bae Jun, and Sang Mun Jeong*,†**

*Department of Chemical Engineering, Chungbuk National University,
1 Chungdae-ro, Seowon-gu, Cheongju, Chungbuk 28644, Korea
**School of Environmental Engineering, Chungbuk National University,
1 Chungdae-ro, Seowon-gu, Cheongju, Chungbuk 28644, Korea
(*Received 15 June 2016 • accepted 20 November 2016*)

Abstract—Porous nano-flake-like α-$Co(OH)_2$ thin films were prepared by electro-deposition on graphene nanosheets (GNS) and functionalized f-GNS at 1.0 V. The functionality of hydrophilic functional groups was increased by acid treatment to enhance electrode wettability and improve the compatibility between the electrode and the electrolyte. Hydrophilic functional groups can act as anchoring sites for the precursors, enabling $Co(OH)_2$ to more grow easily on an f-GNS electrode. The density and thickness of the α-$Co(OH)_2$ deposition on the f-GNS electrode (13.1 μm) was greater than that on the GNS (12.3 μm) electrode. The specific discharge capacitance of the α-$Co(OH)_2$/f-GNS electrode decreased from an initial value of 2,149 $mFcm^{-2}$ to 1,944 $mFcm^{-2}$ over 1000 cycles, demonstrating the retention of 90% of its discharge capacitance. A hybrid capacitor was also assembled to evaluate the characteristics of a two-electrode system using α-$Co(OH)_2$/f-GNS as the cathode. The power and energy densities of the $Co(OH)_2$/f-GNS supercapacitor are 1,137 Wkg^{-1} and 43 $Whkg^{-1}$ at 8 $mAcm^{-2}$, respectively.

Keywords: Supercapacitor, α-$Co(OH)_2$, Graphene, Functionalized Graphene, Hybrid Asymmetric Supercapacitor

INTRODUCTION

Current advances in supercapacitor technology have generated further research into the design of large-scale power systems, such as those needed for electric vehicles and energy storage. Supercapacitors provide high power density over long-term cycles and exhibit rapid charging time and chemical stability; moreover, they occupy a small space and can be fabricated at a low cost [1-3].

Supercapacitors can be divided into two general types, electric double-layer capacitors (EDLCs) and pseudocapacitors, based on the type of electrode materials used for their manufacture. Electrodes used for EDLCs are generally thin coatings applied to a conducting metallic current collector. Electrode performance is determined by several factors, such as a high specific area, good porosity, and low internal resistance to the transport of electrical charge [4,5]. However, EDLCs tend to have an energy density (typically 10 $Whkg^{-1}$) lower than that of lithium ion batteries; therefore, novel materials need to be developed if energy and power densities of supercapacitors and pseudocapacitors are to be improved.

Pseudocapacitors store electrical energy faradaically by electron charge transfer between electrode and electrolyte. This is accomplished through electro-sorption, redox reaction, and intercalation processes. Pseudocapacitors composed of transition metal oxides or hydroxides such as MnO_2, $Ni(OH)_2$, RuO_2, and $Co(OH)_2$ have a higher specific capacitance than EDLC [6-9]. Although RuO_2 exhibits very high specific capacitance, its commercialization for supercapacitors is not promising because of high cost, thus indicating the need to identify other materials suitable for use as pseudocapacitor electrodes.

$Co(OH)_2$ is one of the better alternatives for use in supercapacitors because its faradaic reactions exhibit high activity, and it has high energy and high power density [9-12]. $Co(OH)_2$ has a layered structure with large interlayer spacing and high conductivity and it exhibits excellent electrochemical properties. In addition, $Co(OH)_2$ is advantageous because of its low cost and abundance in nature. Therefore, it offers great promise for commercial application for energy storage.

To reduce the cost of supercapacitors, various methods have been proposed for preparing pseudocapacitive materials, such as sol-gel [13], hydrothermal [14], microwave-assisted [15], and electro-deposition [16] methods. Among these, the electro-deposition method is currently of greatest significance and interest for industrial application because of its low cost, simple process, and the inherent ability to control the weight and/or thickness of metal oxides or hydroxides deposited during electrode preparation [17,18].

In this work, in order to obtain high specific capacitance of the supercapacitor, $Co(OH)_2$ was obtained by electro-deposition on the graphene nano-sheets (GNS) or functionalized GNS (f-GNS) in a solution of $Co(NO_3)_2 \cdot 6H_2O$ dissolved in a 1 : 1 vol% solution of H_2O and ethanol. The functionality of the prepared supercapacitors was investigated and the hybrid asymmetric supercapacitor tested using a two-electrode system was placed into 1 M KOH electrolyte.

†To whom correspondence should be addressed.
E-mail: smjeong@chungbuk.ac.kr

EXPERIMENTAL

1. Preparation of f-GNS

Commercial graphene nanosheet (GNS, xGnP-M-5, Enanotect Industry, Ltd.) was used to prepare the functionalized-graphene nanosheet (f-GNS) by following the acid treatment described elsewhere [19]. In this method, 5 g of GNS was suspended in an acid solution prepared by mixing nitric acid (HNO_3, 70%, Merck) and sulfuric acid (H_2SO_4, 98%, SAMCHUN) at a volume ratio of 1 : 3. After stirring vigorously for a few minutes the obtained solution was sonicated in a JEIOTECH US-05 ultrasonic bath for 10 min. The resulting suspension was heated to 134 °C for 20 min and cooled to room temperature under vigorous stirring before further sonication for 20 min and rinsing with deionized water to a final solution pH of 7. A dark brown f-GNS powder was obtained by freeze-drying the suspension under vacuum.

2. Preparation of GNS and f-GNS Electrodes

The GNS and f-GNS slurries used for electrode fabrication were prepared by mixing GNS or f-GNS powder with acetylene black and polyvinylidene fluoride (PVdF) at a mass ratio of 100 : 15 : 10 in N-methyl pyrrolidinone (NMP). The slurry was then cast onto a Ti-mesh and dried at 80 °C in air for 30 min to produce working electrodes that had an active area of 2 cm^2.

3. Electro-deposition of α-$Co(OH)_2$ on GNS and f-GNS Electrodes

Pseudocapacitors were prepared by electro-deposition of α-$Co(OH)_2$ onto GNS or f-GNS electrodes using chronoamperometric techniques. Chronoamperometry was used to deposit $Co(OH)_2$ onto the GNS or f-GNS electrodes electrochemically. Optimal electro-deposition voltage was determined from cyclic voltammetry (CV) analysis before and during electro-deposition. Fig. 1 shows the CV curves for 0.1 M $Co(NO_3)_2 \cdot 6H_2O$ mixed with 1 : 1 vol% water-ethanol anhydrate solution on GNS and f-GNS electrode. The potential was scanned from 0 to −1.5 vs. Ag/AgCl (in 3 M KCl) as the reference at a scan rate of 5 mVs^{-1}. When the potential is swept in the negative direction, a sharp increase in the reduction current takes place at −0.65 V for both GNS and f-GNS electrodes due to the electrochemical reduction of NO_3^- on the surface of the carbon materials. A broad current peak with the GNS electrode appears at −1.0 V due to diffusion limitation and then a dramatic increase in the current is probably due to the formation of hydrogen bubble. Under these conditions, the electrodeposition process of $Co(OH)_2$ most likely includes the electrochemical and precipitation reaction expressed below [21]:

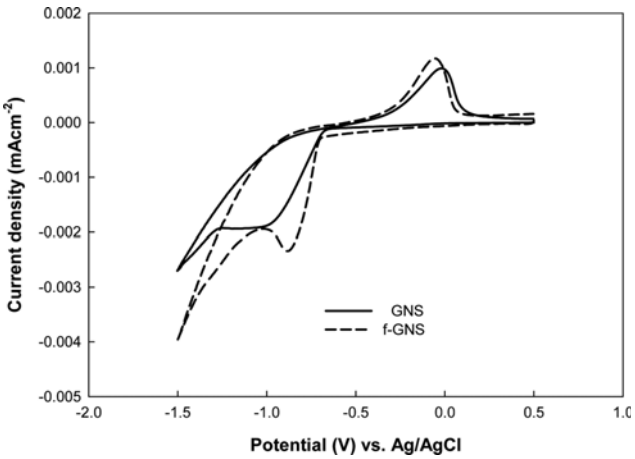

Fig. 1. Cyclic voltammetry curves of GNS and f-GNS in 0.1 M $Co(NO_3)_2 \cdot 6H_2O$ solution at 5 mVs^{-1} scan rate.

$$NO_3^- + 7H_2O + 8e^- \rightarrow NH_4^+ + 10OH^- \quad (1)$$

$$Co^{2+} + 2OH^- \rightarrow Co(OH)_2 \quad (2)$$

When electric current passes through the electrolyte containing $Co(NO_3)_2$, nitrate ions are reduced on the cathodic surface to produce hydroxide ions (OH^-). The generation of OH^- at the cathode raises the local pH, resulting in the precipitation of $Co(OH)_2$ onto the electrode surface [21,22].

A cathodic peak at −0.9 V and a following shoulder are observed with the f-GNS electrode, which might be due to the participation of hydroxyl functional groups on the surface of f-GNS in the electrode reaction. Also, the current density of the f-GNS is higher than that of the GNS, indicating that a greater amount of $Co(OH)_2$ is deposited on the f-GNS electrode [20]. During the reverse scan to the positive direction, the re-oxidation peak appears around 0 V vs. Ag/AgCl due to the oxidation process of reaction (1).

Based on this observation, electro-deposition experiments were performed using a constant potential of −1.0 V against the Ag/AgCl reference electrode for 2 h. The electro-deposition area of the electrodes used was 4 cm^2. After deposition, the prepared α-$Co(OH)_2$/GNS and α-$Co(OH)_2$/f-GNS electrodes were washed with distilled water several times and dried at 80 °C for 30 min.

4. Material Characterization and Electrochemical Measurements

Morphologies of the prepared GNS, f-GNS, $Co(OH)_2$/GNS, and $Co(OH)_2$/f-GNS electrode were characterized by field-emission scanning electron microscopy (FE-SEM; LEO-1530, Carl Zeiss). The functional groups on the carbon materials were analyzed by Fourier transform infrared (FT-IR) spectrophotometer (Nicolet IR 200, Thermo scientific Co. USA). X-ray photoelectron spectroscopy (XPS) on the ESCALAB 210 spectrometer (VG Science, UK) and electrochemical measurements were made in a three-electrode electrochemical cell using 1 M KOH aqueous as the electrolyte. In this cell, $Co(OH)_2$/GNS and $Co(OH)_2$/f-GNS electrodes are used as the working electrodes, a graphite rod as the counter electrode and Ag/AgCl as the reference electrode. Cyclic voltammogram (CV) and galvanostatic charge-discharge measurements were all performed using an Autolab electrochemical workstation (PGSTAT 302N, Netherlands).

5. Preparation of Asymmetric Supercapacitor

The asymmetric supercapacitor was prepared in a two-electrode beaker-type cell. The α-$Co(OH)_2$/f-GNS electrodes were used as positive electrodes and activated carbon as the negative electrode. 1 M KOH was used as the electrolyte and separator was used to prevent short-circuits across the electrodes.

RESULTS AND DISCUSSION

The functionalization of GNS was evident by FT-IR analysis as

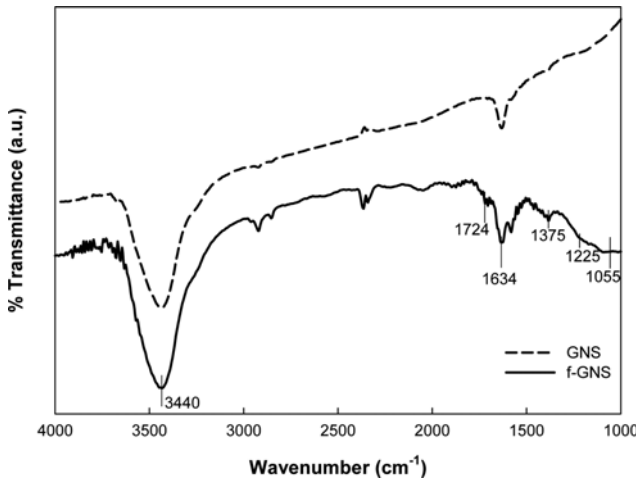

Fig. 2. FT-IR spectra of GNS and f-GNS powders.

shown in Fig. 2. In the FT-IR spectrum of the GNS, the peaks at 3,440 and 1,634 cm^{-1} are attributed to -OH stretch and aromatic C=C vibration, respectively. Upon functionalization of the GNS, new absorption bands appear at 1,724 cm^{-1} (C=O stretch), 1,375 cm^{-1} (C-OH stretch), 1,225-1,055 cm^{-1} (C-O stretch), respectively, indicating the existence of oxygen-containing functional groups on the surface of f-GNS [23-25]. The functional groups in f-GNS have dual roles. First, these hydrophilic groups enhance the wettability of the electrode, improving compatibility between the electrode and the electrolyte. Second, these functional groups can act as anchoring sites for precursors, making it easier for $Co(OH)_2$ to be deposited on f-GNS electrodes than GNS electrodes. Therefore, more $Co(OH)_2$ will be deposited on the surface of f-GNS electrodes than on non-functionalized GNS.

XPS was used to discuss the chemical and structural state of the electrode materials. The C1s core level XPS spectra of GNS and f-GNS are shown in Fig. 3(a) and (b). These spectra showed four main peaks, corresponding to the carbon atoms in different functional groups. The characteristic peaks at 284.4, 285.9, 287.8, and 288.8 eV are attributed to unoxidized graphite carbon (C-C), hydroxyl carbon (C-O), carbonyl carbon (C=O), and carboxylate carbon (O-C=O), respectively [26,27]. The typical $Co2p_{3/2}$ and satellite XPS spectra of $Co(OH)_2$ deposited on α-$Co(OH)_2$/GNS and α-$Co(OH)_2$/f-GNS electrodes are shown in Fig. 3(a) and (b), respectively. The binding energy value of 780.3 eV for $Co2p_{3/2}$ was consistent with the data recently reported for Co-containing oxidase. The Co $2p_{3/2}$ spectra are complex because they exhibit two spin-orbit doublets and several shake-up satellites. The spin-orbit doublet is characterized by binding energy of 780.3 eV in the Co $2p_{3/2}$ core levels, in conjunction with a small shake-up satellite peak at 785.5 eV, which is a characteristic of Co^{3+}. The broader spin-orbit doublets with binding energy of 781.9 eV and strong shake-up sat-

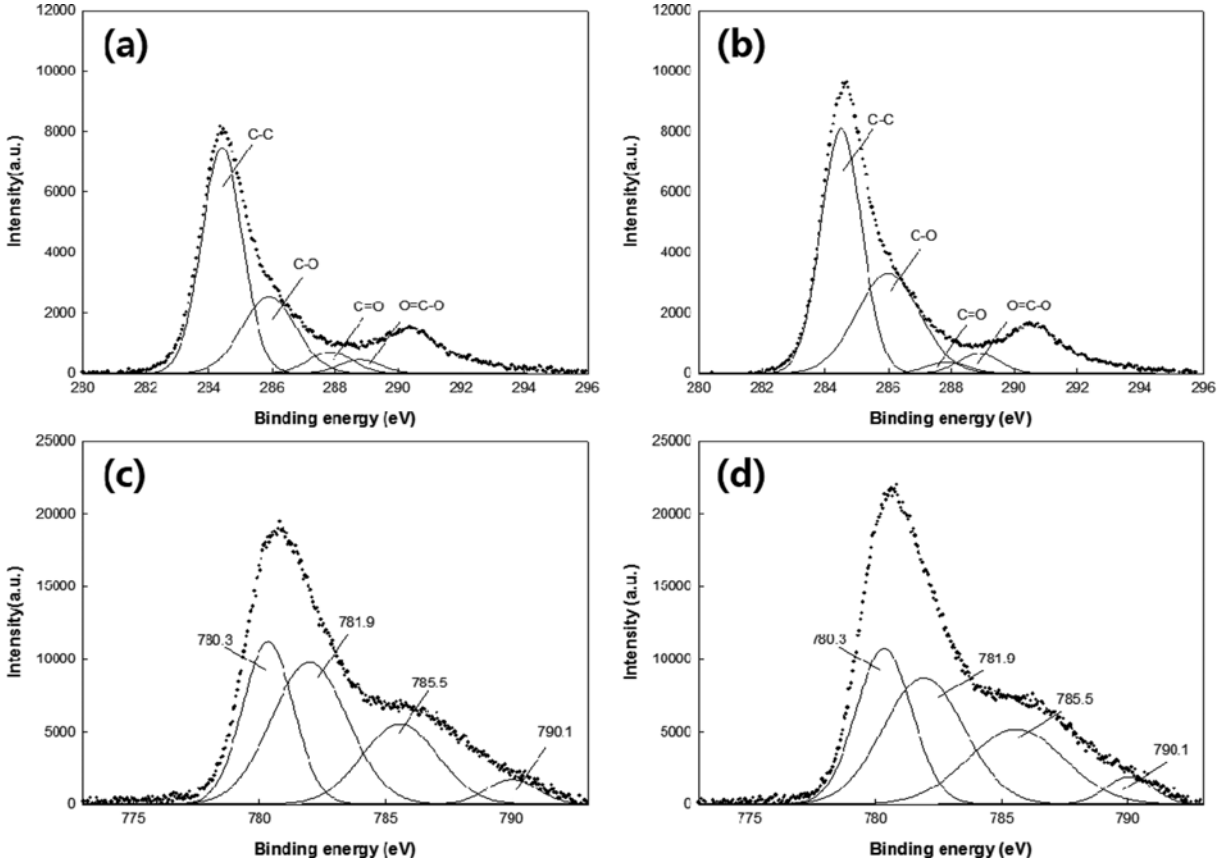

Fig. 3. C1s XPS spectra for (a) GNS and (b) f-GNS electrode, and Co $2p_{3/2}$ XPS spectra for (c) α-$Co(OH)_2$/GNS and (d) α-$Co(OH)_2$/f-GNS electrodes.

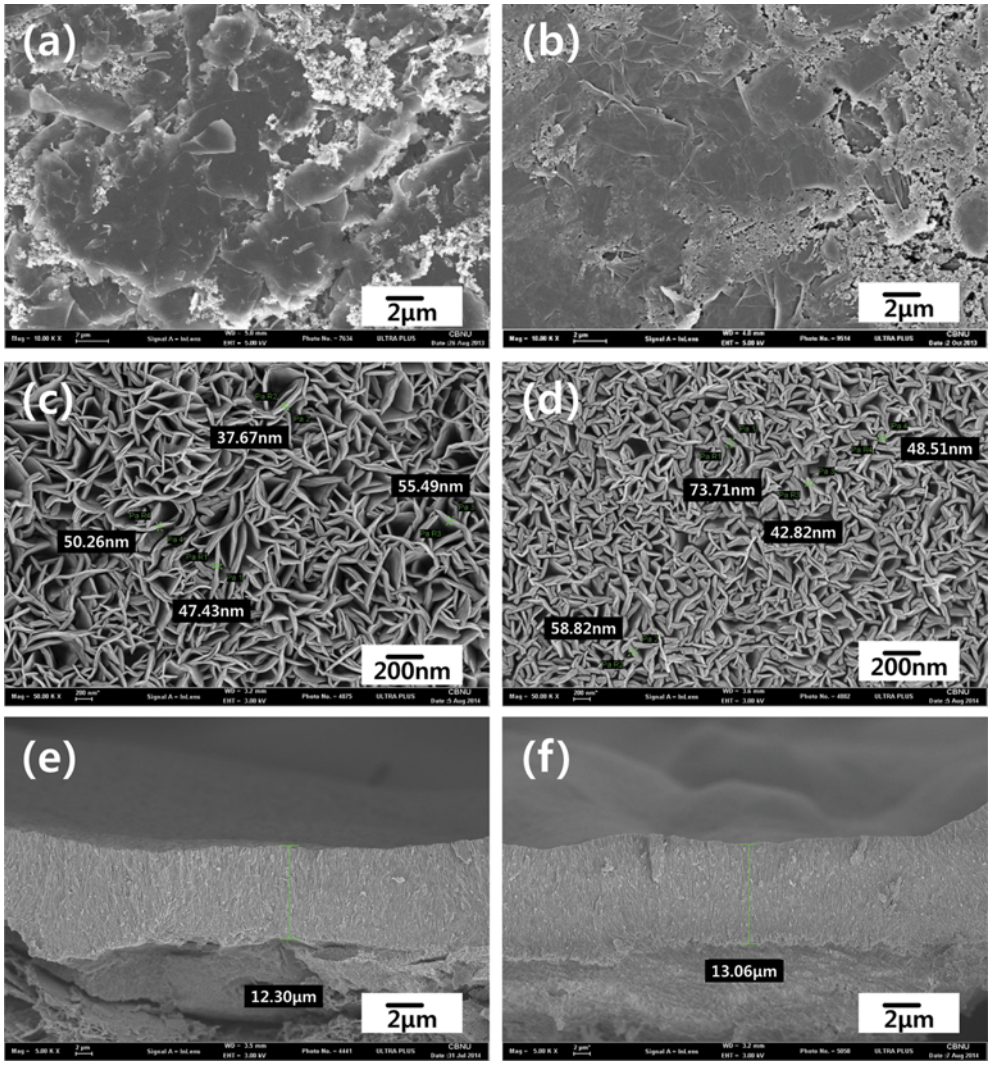

Fig. 4. Surface FE-SEM images of (a) GNS, (b) f-GNS, (c) α-$Co(OH)_2$/GNS, (d) α-$Co(OH)_2$/f-GNS electrodes and cross section FE-SEM images of (e) α-$Co(OH)_2$/GNS, (f) α-$Co(OH)_2$/f-GNS electrodes.

ellites at 790.1 eV were assigned to Co^{2+}.

FE-SEM images of the GNS, f-GNS, α-$Co(OH)_2$/GNS, and α-$Co(OH)_2$/f-GNS electrodes are shown in Fig. 4. The GNS and f-GNS electrodes were composed of a large number of stacked graphene sheets, as can be seen in Fig. 4(a) and (b). The surface and cross-sectional FE-SEM images of α-$Co(OH)_2$/GNS and α-$Co(OH)_2$/f-GNS electrodes are shown in Fig. 4(c)-(f). As shown in Fig. 4(c) and (d), the surfaces of α-$Co(OH)_2$/GNS and α-$Co(OH)_2$/f-GNS electrodes were covered by nano-flakes of $Co(OH)_2$, where the flake thickness ranges between 30 and 60 nm for α-$Co(OH)_2$/GNS electrodes and between 40 and 80 nm for α-$Co(OH)_2$/f-GNS electrodes, respectively. The denser α-$Co(OH)_2$ flake grew on the surface of f-GNS electrode, indicating that $Co(OH)_2$ was deposited more uniformly or that a greater amount of $Co(OH)_2$ was deposited on the f-GNS electrode. This suggests that depositing $Co(OH)_2$ onto f-GNS electrodes may enhance electrolyte ion accessibility and electron charge transfer at the electrolyte interface. This would lead to thicker α-$Co(OH)_2$ layers and increased density of $Co(OH)_2$ flakes in α-$Co(OH)_2$/f-GNS electrodes, as shown in the cross-sectional images (Fig. 4(e) and (f)). The α-$Co(OH)_2$ thickness of α-$Co(OH)_2$/GNS and α-$Co(OH)_2$/f-GNS electrodes are 12.30 and 13.06 μm, respectively.

Cyclic voltammetry curves for α-$Co(OH)_2$/GNS and α-$Co(OH)_2$/f-GNS electrodes measured at scan rates of 5, 10, and 20 mVs^{-1} are shown in Fig. 5. These curves are generally similar to the rectangular shape that is typical of supercapacitor behavior. They demonstrate the quasi-reversible redox reactions that occur for $Co(OH)_2$ during the potential sweep of the electrode [9]:

$$Co(OH)_2+OH^- \leftrightarrow CoOOH+H_2O+e^- \quad (3)$$

Fig. 5(a) and (b) indicate that the electrochemical current of the α-$Co(OH)_2$/f-GNS electrode is higher than that of α-$Co(OH)_2$/GNS, and that peak current increased in line with the increase in the scan rate. In addition, the CV curves exhibits rectangular shape, which shows the occurrence of supercapacitive behavior. These results suggest that more OH^- was in contact with the α-$Co(OH)_2$/f-GNS electrode because of the higher number of hydrophilic functional groups and the greater density of $Co(OH)_2$ flakes

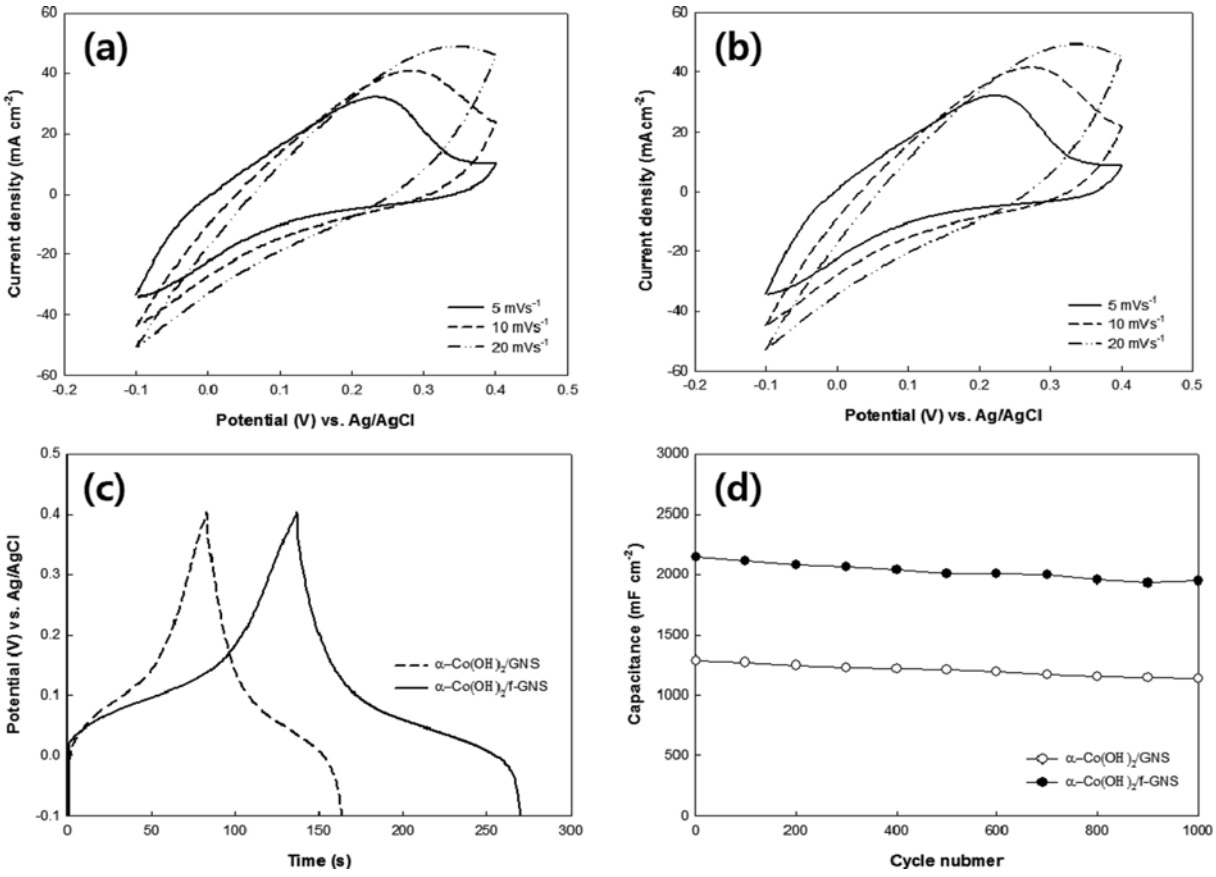

Fig. 5. Cyclic voltammetry curves of the (a) α-Co(OH)$_2$/GNS, (b) α-Co(OH)$_2$/f-GNS electrodes, (c) galvanostatic charge-discharge curves, and (d) cycling performance of α-Co(OH)$_2$/GNS and α-Co(OH)$_2$/f-GNS electrodes.

grown on the α-Co(OH)$_2$/f-GNS electrodes.

An electrode material for supercapacitor should have not only a high mass specific capacitance, C_M (Fg^{-1}) but also a high electrode specific capacitance, C_E (Fcm^{-2}), which is practically important in the electro-deposition technique [28]. In this work, the electrode specific capacitance, C_E, was measured based on the electro-deposition area. The electrode specific capacitance (C_E) values were calculated from the CV curves at different scan rates using the following equation [29]:

$$C_E = \frac{\int IdV}{2 \times v \times A \times \Delta V} \quad (4)$$

where $\int IdV$ is the integrated area of the CV curve, v is the potential scan rate, A is the area of the electrode, and ΔV is the range of the potential applied. Using this formula, the specific capacitance of α-Co(OH)$_2$/f-GNS electrode at 5 mVs^{-1} were measured as 2,944 $mFcm^{-2}$, indicating that α-Co(OH)$_2$/f-GNS electrodes have excellent specific capacitance. In addition, the SC values of the α-Co(OH)$_2$/f-GNS electrode are 2,108 and 1,335 $mFcm^{-2}$ at the 10 and 20 mVs^{-1} scan rates, respectively.

Fig. 5(c) shows the galvanostatic charge-discharge curves of α-Co(OH)$_2$/GNS and α-Co(OH)$_2$/f-GNS electrodes in a potential window between −1.0 and 0.4 V at 8 $mAcm^{-2}$. The charge-discharge curves exhibit a symmetric shape, which indicates good electrochemical capacitive characteristics and the presence of reversible redox reactions. The curves also show that α-Co(OH)$_2$/f-GNS electrode has a longer charge-recharge cycle than α-Co(OH)$_2$/GNS electrodes.

The capacitance (C_E) of the galvanostatic discharge curve at a constant current density was calculated according to the following equation [6]:

$$C_E = \frac{I \times t}{\Delta V \times A} \quad (5)$$

where I is the current applied to the charge-discharge cycle, t is the time of discharge, ΔV is the potential range, and A is the area of the coated material. Using this formula, specific capacitance values for the α-Co(OH)$_2$/GNS and α-Co(OH)$_2$/f-GNS electrodes are calculated to be 1,340 and 2,384 $mFcm^{-2}$, respectively.

Cycling performance of the supercapacitor material was investigated by measuring discharge retention over 1000 charge-discharge cycles. Fig. 5(d) shows that cycling reduced the discharge capacitance of the α-Co(OH)$_2$/GNS electrodes from 1,285 to 1,139 $mFcm^{-2}$ and α-Co(OH)$_2$/f-GNS electrodes from 2,149 to 1,944 $mFcm^{-2}$. This means that the α-Co(OH)$_2$/GNS and α-Co(OH)$_2$/f-GNS electrodes, respectively, retain 89% and 91% of their ability to discharge over a long period of time. It is this excellent electrochemical activity and cycling stability of the α-Co(OH)$_2$/f-GNS electrodes that makes them potentially useful as asymmetric supercapacitors.

Results of further analysis of the electrochemical properties of

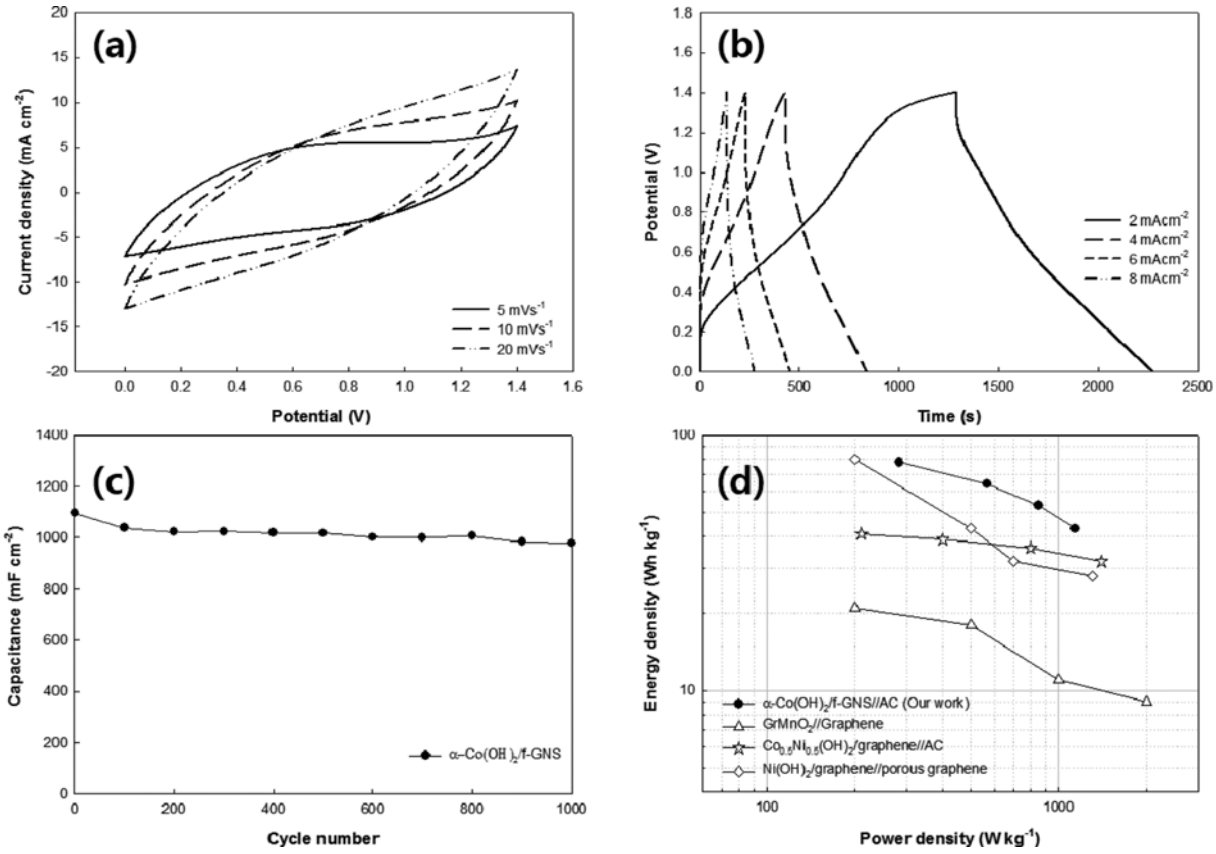

Fig. 6. Electrochemical performance of the hybrid α-Co(OH)$_2$/f-GNS capacitor in 1M KOH solution. (a) CV curves, (b) galvanostatic charge-discharge curves, (c) cycling performance at 4 mAcm^{-2} current density, and (d) the plots of power and energy density of the asymmetric supercapacitor recently reported in the literature [27-29].

α-Co(OH)$_2$/f-GNS electrodes are shown in Fig. 6. Fig. 6(a) shows the results of CV analysis across the range 0-1.4 V for cells containing activated carbon anodes and α-Co(OH)$_2$/f-GNS cathodes in a 1 M KOH electrolyte. The CV curves were rectangular and similar to typical EDLC curves that are based on non-faradaic reactions over the range varying from −1.0 to 0 V, and showed capacitances of 854, 573, and 355 mFcm^{-2} at 5, 10, and 20 mVs^{-1}, respectively, for the hybrid α-Co(OH)$_2$/f-GNS asymmetric supercapacitor.

Fig. 6(b) shows charge-discharge performance across the galvanic potential range 0-1.4 V. Although a region of non-linearity in the discharge curves is observed at a lower current density (2 mAcm^{-2}), the near symmetry of the curves confirms that the supercapacitor can store a highly reversible electrochemical charge. Fig. 6(c) shows the cycling performance of α-Co(OH)$_2$/f-GNS asymmetric supercapacitors at a current density of 4 mAcm^{-2} over the range 0-1.4 V. Capacitance was found to drop from 1,097 mFcm^{-2} at the initial cycle to 979 mFcm^{-2} by the 1,000th cycle, indicating 90% retention.

Ragone plots relating energy to power densities are an efficient way to evaluate the capacitive performance of supercapacitors (Fig. 6(d)). The power density (P) and energy density (E) used in the Ragone plots for the asymmetric supercapacitor were calculated from the following equations [3,6,18]:

$$P = \frac{1}{2}IV \quad (6)$$

$$E = \frac{1}{2m}CV^2 \quad (7)$$

where I is the specific current (Ag^{-1}), V is the potential range of the supercapacitor, and C is the capacitance of the hybrid supercapacitor.

Results were compared against those of other asymmetric supercapacitors referenced from literature [30-32]. It was found that 1.6 V Ni(OH)$_2$/graphene//porous graphene asymmetric supercapacitors exhibit an energy density of 77.8 Whkg^{-1} at a power density of 174.7 Wkg^{-1} and are still capable of retaining 13.5 Whkg^{-1} at a power density of 15.2 kWkg^{-1} [30]. Also, 1.4 V Co$_{0.5}$Ni$_{0.5}$(OH)$_2$/graphene/CNTs//AC supercapacitors exhibited an energy density of 41 Whkg^{-1} at a power density of 210 Wkg^{-1} [31]. In comparison, the 1.4 V α-Co(OH)$_2$/f-GNS//AC asymmetric supercapacitor has power densities of 284, 569, 853, and 1,137 Wkg^{-1} and energy densities of 78, 64, 53, and 43 Whkg^{-1} at 2, 4, 6, and 8 mAcm^{-2}, respectively. This suggests that the energy and power densities of α-Co(OH)$_2$/f-GNS asymmetric supercapacitors are higher than those of other metal-hydroxide asymmetric supercapacitors reported in literature [30-32], making them attractive alternatives for use as a hybrid capacitor.

CONCLUSIONS

α-Co(OH)$_2$ nano-flakes were successfully deposited on GNS or

f-GNS substrates at −1.0 V, with greater amounts deposited onto the f-GNS electrode. The discharge capacitance decreased from 1,285 to 1,139 $mFcm^{-2}$ for the α-$Co(OH)_2$/GNS and from 2,149 $mFcm^{-2}$ to 1,944 $mFcm^{-2}$ for α-$Co(OH)_2$/f-GNS electrodes over 1,000 cycles. The α-$Co(OH)_2$/GNS showed 89% retention of discharge capacitance, and α-$Co(OH)_2$/f-GNS electrodes showed 91% retention. In a two-electrode system using the α-$Co(OH)_2$/f-GNS as a cathode, the specific discharge capacitance decreased from 1,097 to 979 $mFcm^{-2}$ over the 1000 cycles, representing a capacitance retention of 90%. Power and energy densities of the $Co(OH)_2$/f-GNS supercapacitor were calculated as 1,137 and 43 $Whkg^{-1}$ at 8 mA cm^{-2}. These results show that acid treatment of GNS creates an activated substrate (f-GNS) with an increased number of functional groups on the surface, promoting greater deposition of α-$Co(OH)_2$ and indicating that α-$Co(OH)_2$/f-GNS electrodes possess excellent electrochemical properties.

ACKNOWLEDGEMENTS

This work was funded by the MOTIE/KIAT (R0004144), and also partly supported by a National Research Foundation of Korea (NRF) grant, funded by the Korea government (MISP) (2015M2B2A9030532).

REFERENCES

1. C. Portet, P. L. Tabema, P. Simon, E. Flahaut and C. Laberty-Robert, *Electrochim. Acta*, **50**, 4174 (2005).
2. H. Luo, L. Zheng, L. Lei, D. Zhang, J. Wu and J. Yang, *Korean J. Chem. Eng.*, **31**, 712 (2014).
3. T. Toomin, T. Thomberg, H. Kurig, A. Jämes and E. Lust, *J. Power Sources*, **280**, 667 (2015).
4. A. B. Fuertes and M. Sevilla, *Carbon*, **94**, 41 (2015).
5. P. K. Kalambate, R. A. Dar, S. P. karna and A. K. Srivastava, *J. Power Sources*, **276**, 262 (2015).
6. L. Li, M. Z. A. Hu, N. An, Y. Y. Yang, Z. M. Li and H. Y. Wu, *J. Phys. Chem. C*, **118**, 22865 (2014).
7. H. B. Li, M. H. Yu, F. X. Wang, P. Liu, Y. Liang, J. Xiao, C. X. Wang, Y. X. Tong and G. W. Yang, *Nature Commun.*, 4:1894, 1 (2013).
8. C. C. Hu and W. C. Chen, *Eelctrochim. Acta*, **49**, 3469 (2004).
9. L. Cao, F. Xu, Y. Y. Liang and H. L. Li, *Adv. Mater.*, **16**, 1853 (2004).
10. C. yuan, L. Hou, L. Shen, D. Li, F. Zhang, C. Fan, J. Li and X. Zhang, *Electrochim. Acta*, **56**, 115 (2010).
11. J. K. Chang, C. M. Wu and I. W. Sun, *J. Mater. Chem.*, **20**, 3729 (2010).
12. Z. Chen, Y. Chen, C. Zuo, S. Zhou, A. G. Xiao and A. X. Pan, *Bull. Mater. Sci.*, **36**, 239 (2013).
13. Y. Liu, N. Wang, C. Yang and W. Hu, *Ceram. Int.*, **42**, 11411 (2016).
14. D. Li, F. Yu, Z. Yu, X. Sun and Y. Li, *Mater. Lett.*, **158**, 17 (2015).
15. F. Zhou, Q. Liu, J. Gu, W. Zhang and D. Zhang, *Electrochim. Acta*, **170**, 328 (2015).
16. H. J. Lee, E. M. Jin and S. M. Jeong, *Korean Chem. Eng. Res.*, **54**, 157 (2016).
17. H. Ashassi-Sorkhabi, P. L. Badakhshan and E. Asghari, *Chem. Eng. J.*, **299**, 282 (2016).
18. T. Peng, H. Wang, H. Yi, Y. Jing, P. Sun and X. Wang, *Electrochim. Acta*, **176**, 77 (2015).
19. C. C. Hu, J. C. Chen and K. H. Chang, *J. Power Sources*, **221**, 128 (2013).
20. E. M. Garcia, V. F. C. Lins and T. Matencio, *Intech. Chapter*, **5**, 101 (2013).
21. T. Zhao, H. Jiang and J. Ma, *J. Power Sources*, **196**, 860 (2011).
22. C. M. Chen, J. Q. Huang, Q. Zhang, W. Z. Gong, Q. H. Yang, M. Z. Wang and Y. G. Yang, *Carbon*, **50**, 659 (2012).
23. M. Naebe, J. Wang, A. Amini, H. Khayyam, N. Hameed, L. H. Li, Y. Chen and B. Fox, *Sci. Reports*, 4:4375, 1 (2014).
24. P. Dong, Y. Wang, L. Guo, B. Liu, S. Xin, J. Zhang, Y. Shi, W. Zeng and S. Yin, *Nanoscale*, **4**, 4641 (2012).
25. C. Peng, J. Jin and G. Z. Chen, *Electrochim. Acta*, **53**, 525 (2007).
26. J. Yang, H. Liu, W. N. Martens and R. L. Frost, *J. Phys. Chem. C*, **114**, 111 (2009).
27. C. M. Wu, C. Y. Fan, I. W. Sun, W. T. Tsai and J. K. Chang, *J. Power Sources*, **196**, 7828 (2011).
28. Z. Fan, J. Yan, J. Zhi, Q. Zhang, T. Wei, J. Feng, M. Zhang, W. Qian and F. Wei, *Adv. Mater.*, **22**, 3723 (2010).
29. A. A. Ensafi, N. Ahmadi and B. Rezaei, *RSC Adv.*, **5**, 91448 (2015).
30. J. Yan, Z. Fan, W. Sun, G. Ning, T. Wei, Q. Zhang, R. Zhang, L. Zhi and F. Wei, *Adv. Funct. Mater.*, **22**, 2632 (2012).
31. Y. Cheng, H. Zhang, C. V. Varanasi and J. Liu, *Energy Environ., Sci.*, **6**, 3314 (2013).
32. J. Chang, M. Jin, F. Yao, T. H. Kim, V. T. Le, H. Yue, F. Gunes, B. Li, A. Ghosh, S. Xie and Y. H. Lee, *Adv. Funct. Mater.*, **23**, 5074 (2013).